frontiers | Frontiers in Physics

TYPE Original Research
PUBLISHED 04 May 2023
DOI 10.3389/fphy.2023.1181343

OPEN ACCESS

EDITED BY
Bin Zhang,
Sichuan University, China

REVIEWED BY
Liguo Wang,
Xi'an Technological University, China
Chaoliang Ding,
Luoyang Normal University, China

*CORRESPONDENCE
Xiang'e Han,
xehan@mail.xidian.edu.cn

RECEIVED 07 March 2023
ACCEPTED 18 April 2023
PUBLISHED 04 May 2023

CITATION
Miao Z, Zhang P, Lu F, Han X and Li Q (2023), Light field analysis for modeling and transmission characteristics of partially coherent light-emitting diodes. *Front. Phys.* 11:1181343.
doi: 10.3389/fphy.2023.1181343

Light field analysis for modeling and transmission characteristics of partially coherent light-emitting diodes

Zhifang Miao[1], Pengfei Zhang[2], Fang Lu[2], Xiang'e Han[2]* and Qiwei Li[2]

[1]School of Telecommunication Engineering, Xidian University, Xi'an, China, [2]Photodetection Theory and Application Laboratory, School of Physics, Xidian University, Xi'an, China

When analyzing the transmission characteristics of LEDs for long-distance lighting and communication applications, the light field is commonly assumed to be fully incoherent. However, in reality, the LED light source emits partially coherent light with a spatial coherence length on the order of microns. This paper is based on the generalized higher-order Lambert model of LEDs and aims to construct a Gaussian-Schell model for the LED beam (LED-GSM) on the near-field source plane, with a half-power angle of no more than 10°. Utilizing the cross-spectral density function transmission theory for partially coherent light, this paper provides the LED-GSM model's spatial coherence length and beam radius at different distances and designs an experiment for measuring the spatial coherence length of LED beams. Experimental measurements of the spatial coherence length and beam spot size of LED beams at different distances are carried out using a Thorlabs LED528EHP light source. The experimental results match well with the theoretical simulations of the LED-GSM model, thus validating its effectiveness. Then, the proposed LED-GSM model is utilized to investigate the long-distance transmission characteristics of partially coherent narrow-beam LED light. Simulation results indicate that the spatial coherence length of the LED light field can reach tens to hundreds of millimeters over transmission distances of several kilometers. The beam radius is much smaller than that of the beam radius based on the fully incoherent model, and the beam intensity distribution also displays distinct differences.

KEYWORDS

LEDs (light-emitting diodes), narrow beam angle, Gaussian-Schell model, long-distance, spatial coherence, beam expansion

1 Introduction

The high electro-optical efficiency, strong radiation power, long lifespan, and low cost of LEDs have made them widely used in various fields, including lighting, display, and optical communication. In the past decades, the coherence of light fields has been studied in the context of LED applications such as optical communication [1,2], digital holographic displays [3], and interferometric measurements [4,5]. Measurements of the spatial coherence of LED light fields indicate that they are not completely incoherent, but instead, contain partially coherent light with spatial coherence lengths varying from a few to several tens of micrometers [6,7]. The size of the spatial coherence length is linked to

the LED light source material and the structure of the emitting chip [8]. Mehta et al. [9] conducted a comprehensive investigation on the spectral and temporal coherence of LEDs. Lin et al. [10] experimentally determined the spatial coherence length of LEDs with various emitting chip shapes over transmission distances of several meters. The findings suggest that with an increase in transmission distance, the spatial coherence length of the optical field will extend to the millimeter scale. The spatial coherence of partially coherent light from LEDs [11] at close range is often overlooked and assumed to be completely incoherent[12]. Nonetheless, its partial coherence cannot be disregarded in long-distance transmission. With the growing prominence of decoherence properties in laser transmission theory[13], there is an increasing focus on analyzing the spatial coherence characteristics of partially coherent optical transmission theories, including the typical Gaussian-Schell model (GSM)[14]. This theoretical approach is capable of dealing with partially coherent as well as fully incoherent light sources [15], which provides a theoretical basis for investigating the spatial coherence of partially coherent LED light in a vacuum environment.

With the advancements in LED materials and light source design [16], LED light sources that exhibit excellent directionality and high power [17] have become a fundamental component for long-distance lighting and optical communication applications. Currently, LED light source systems that encapsulate light-emitting chips and use focused lenses are often considered as fully incoherent light sources in research on communication channel characteristics. However, the transmission characteristics of partially coherent light fields suggest that [18], during long-distance transmission, the spatial coherence and beam radius of the light field differ from those of fully incoherent light. Therefore, it is crucial to investigate the partial coherence properties of LED light using the theory of partially coherent light transmission.

Based on the near-field measurement results of the lateral spatial coherence length and beam radius of LED, a partially coherent light model for LEDs with micro-scale spatial coherence length at the near-source plane is developed through theoretical simulations and experimental measurements. During the beam propagation, the study examines the impact of factors such as spatial complex coherence, source size, and transmission distance on the spatial coherence length and beam radius of the light field on the observation plane.

2 LED-GSM model and transmission theory

2.1 Light field of LED

The illuminance distribution of LED is generally described using the generalized Lambertian model. (H and M, 2008)

$$E_{Lam}(\mathbf{r},z)=\frac{m+1}{2\pi z^2}E_0\cos^{m+3}(\theta)=\frac{m+1}{2\pi z^2}E_0\left(1+\frac{\mathbf{r}^2}{z^2}\right)^{-\frac{m+3}{2}} \quad (1)$$

Where z denotes the distance between the light source and the observation plane, $\mathbf{r}(x,y)$ represents the position vector of a point on the z plane, and E_0 corresponds to the radiance emitted by the center of the light source. The polar angle of the location with respect to the LED is denoted by θ, $\theta=\arctan(r/z)\times 180/\pi$. m is the Lambertian mode number and $m>0$. The mode number is a measure of the directivity of the light beam and is related to the semiangle of the light beam at half power, denoted by $\Phi_{1/2}$, by $m=-\ln(2)/\ln(\cos(\Phi_{1/2}))$.

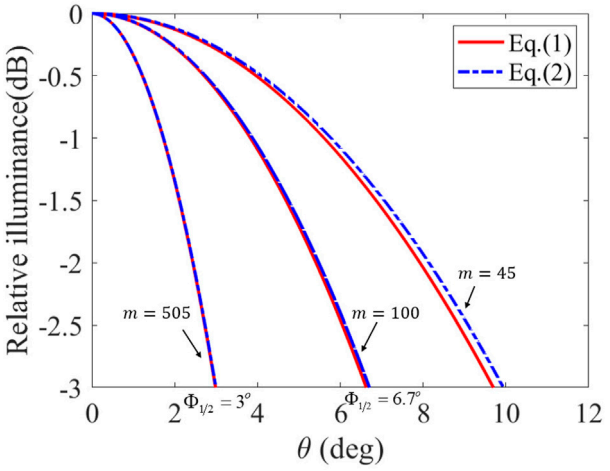

FIGURE 1
The relationship between relative illuminance and θ at different values of m (z = 0.1 m).

Since $\Phi_{1/2}\le 10^o$, the LED near-field radiation can be approximated as a Gaussian distribution [19]. Considering the condition of $\mathbf{r}^2=x^2+y^2\ll z^2$, the Gaussian analytical expression, approximated by expanding $E_{Lam}(\mathbf{r},z)$ using a Taylor series, is represented as

$$E_{Gau}(\mathbf{r},z)=\frac{(m+1)E_0}{2\pi z^2}\exp\left\{-\frac{m}{2}\cdot\frac{\mathbf{r}^2}{z^2}\right\}=\frac{(m+1)E_0}{2\pi z^2}\exp\left\{-\frac{2\mathbf{r}^2}{w^2(z)}\right\} \quad (2)$$

Where $w(z)=2z/\sqrt{m}$ is the radius of the beam waist at the z plane.

Figure 1 shows the relationship between relative illuminance and θ at different values of m. From the curve in the figure, a larger m corresponds to a narrower beam. Commercially available LED lenses can shape the beam of the Lambertian-type LEDs into $\Phi_{1/2}=10^o$, $\Phi_{1/2}=6.7^o$ to $\Phi_{1/2}=3^o$ (H and M, 2008), which correspond to $m=45$,$m=100$ and $m=505$, respectively. Here, it is noted that due to limitations imposed by the experimental equipment, the near-field radiation of the LED can be effectively modeled as a Gaussian distribution when we focus on the range of $m\ge 45$, $\Phi_{1/2}\le 10^o$.

2.2 LED-GSM model

When researching the radiation transmission theory, it is typically required to construct a complex amplitude expression for the outgoing light field. To distinguish z, it is assumed that

the illumination distribution on the z_1 plane follows Gaussian distribution characteristics, where z represents the distance of light transmission. In the case of the LED illumination distribution expressions (1) (2) and the consideration of $\Phi_{1/2} \le 10^o$ and $\mathbf{r}^2 \ll z_1^2$, if the narrow beam light field $E_{Gau}(\mathbf{r}, z_1, t)$ satisfies Gaussian distribution characteristics, then the complex amplitude expression for the observation plane at $z = z_1$ can be expressed as follows:

$$U_{Gau}(\mathbf{r}, z_1, t) = |E_{Gau}(\mathbf{r}, z_1, t)|^{1/2} \exp[-i\phi(\mathbf{r}, t)] = \left[\frac{(m+1)E_0}{2\pi {z_1}^2}\right]^{1/2} \exp\left[-\frac{\mathbf{r}^2}{w^2(z_1)}\right] \exp[-i\phi(\mathbf{r}, t)] \tag{3}$$

Where $U_{Gau}(\mathbf{r}, z_1, t)$ is the scalar optical field, and $\phi(\mathbf{r}, t)$ is satisfied with the random phase on $(-\pi, \pi)$.

By applying the theory of partially coherent light propagation, the spatial coherence of a monochromatic light wave field with a wavelength of λ on any plane in space can be described through the Cross-Spectral Density Function (CSDF). The definition of $W(\mathbf{s}_1, \mathbf{s}_2)$ is as follows:

$$W(\mathbf{s}_1, \mathbf{s}_2) = \langle U(\mathbf{s}_1) U^*(\mathbf{s}_2) \rangle_{st} \tag{4}$$

Where $\mathbf{s}_1$ and $\mathbf{s}_2$ are the position vectors of any two points in the source plane, $_{st}$ denotes the ensemble average. Assuming that the radiation from the LED follows Equation 3, with an amplitude distribution described by a Gaussian model and a spatial coherence distribution that also follows a Gaussian function [20], then the distribution of the CSDF for the light field on the LED's near-source plane at position z_1 follows the definition of the Gaussian-Schell model (GSM), which is commonly abbreviated as LED-GSM. From Equation 3, the expression for the CSDF of a narrow-beam LED on the z_1 plane can be derived.

$$W(\mathbf{s}_1, \mathbf{s}_2, z_1) = \frac{(m+1)E_0}{2\pi {z_1}^2} \exp\left[-\frac{({\mathbf{s}_1}^2 + {\mathbf{s}_2}^2)}{w^2(z_1)}\right] \exp\left[-\frac{(\mathbf{s}_1 - \mathbf{s}_2)^2}{2\sigma^2}\right] \tag{5}$$

where σ is the spatial coherence length of the z_1 plane light field. The larger it is, the better the spatial coherence of the beam, and *vice versa*, the worse the spatial coherence becomes.

After reviewing the literature [6–8], it is evident that the spatial coherence length, σ, of LED emitting chips typically falls within the micrometer range. It is important to take into account the size of the LED light source following processing and optical packaging, as the spatial coherence length of the emitted light on the exit plane generally ranges from several to tens of micrometers. This relationship is closely tied to factors such as the material and size of the LED chip, the divergence angle of the beam, and the emission mode of the light source.

Looking at Figure 1, it becomes apparent that the intensity of the LED follows a Gaussian distribution when z_1 is sufficiently large (e.g., z_1 = 0.1 m, $m \ge 45$). Taking into account the design and dimensions of the LED light source structure, the light plane at a constant value of z_1 can be viewed as the output light field of the entire LED transmission system, referred to as the LED-GSM light source plane. The radius size of the light beam at the light source plane can be defined as $w_s = 1/2w(z_1)$, and Equation 5 can be expressed as

$$W(\mathbf{s}_1, \mathbf{s}_2, z_1) = A \exp\left[-\frac{({\mathbf{s}_1}^2 + {\mathbf{s}_2}^2)}{4w_s^2}\right] \exp\left[-\frac{(\mathbf{s}_1 - \mathbf{s}_2)^2}{2\sigma^2}\right] \tag{6}$$

Where $A = \left(\frac{(m+1)E_0}{2\pi {z_1}^2}\right)$ is the amplitude. From the calculation of Equation 2, as m = 505 and $w_s = 1/2w(z_1 = 0.1)$ = 3mm, the size parameter serves as a reference for selecting the value of w_s in subsequent simulations.

Notably, Equation 6 is the coherent optical field model for the partial coherent light of LED-GSM proposed in this paper, which is valid when $\Phi_{1/2} \le 10^o$ and $\mathbf{r}^2 \ll z_1^2$.

2.3 LED-GSM optical transmission

According to the theory of light transmission in a vacuum for partially coherent light [13,14], under the approximation of the generalized Huygens-Fresnel principle, the CSDF distribution of any two points, such asρ_1 and ρ_2, on the observation plane at z distance from the source plane is given as

$$W(\rho_1, \rho_2, z) = \langle U(\rho_1, z) U^*(\rho_2, z) \rangle_{st} = \left(\frac{k}{2\pi z}\right)^2 \int\int\int\int d^2\mathbf{s}_1 d^2\mathbf{s}_2 W(\mathbf{s}_1, \mathbf{s}_2, z_1) \times \exp\left[ik\frac{(\rho_1 - \mathbf{s}_1)^2 - (\rho_2 - \mathbf{s}_2)^2}{2z}\right] \tag{7}$$

Where $k = 2\pi/\lambda$ is the wave number. λ is the main wavelength of the narrow beam LED. When $\rho_1 = \rho_2 = \rho$, the intensity of light on the observation plane at z distance is obtained as

$$I(\rho, z) = W(\rho, \rho, z) \tag{8}$$

Based on the definition of spatial complex coherence [21], while $\rho_1 = \rho$, $\rho_2 = 0$, the spatial complex coherence of LED-GSM beam can be calculated as Equation 9. Letting $|\mu(\rho_0, 0, z)| = e^{-1}$, the spatial coherence length $\rho_0(z)$ on the observation plane can be found [21]. Based on the definition of the second moment width [22], one can derive an expression for the radius of a beam when it is transmitted in a vacuum.

$$\mu(\rho, 0, z) = \frac{W(\rho, 0, z)}{\sqrt{W(\rho, 0, z) W(\rho, 0, z)}} = \exp\left[-\left(\frac{1}{2\theta_s^2 T(z)} - \frac{1}{8w_s^2 T(z)}\right)\rho^2\right] \exp\left[\frac{ik\rho^2}{2T(z)}\right] \tag{9}$$

$$\rho_0(z) = \left(\frac{1}{2\theta_s^2 T(z)} - \frac{1}{8w_s^2 T(z)}\right)^{-1/2} \tag{10}$$

$$w(z) = \left\{2w_s^2\left[1 + \left(\frac{z}{kw_s\theta_s}\right)^2\right]\right\}^{1/2} \tag{11}$$

Where $T(z) = 1 + \left(\frac{z}{kw_s\theta_s}\right)^2$, and $\frac{1}{\theta_s^2} = \frac{1}{4w_s^2} + \frac{1}{\sigma^2}$ [18], the beam expansion is related to the size of the light source and the spatial coherence length of σ. Under the condition of satisfying the Gaussian model, the beam radius is equal to the spot radius [22]. The spot radius is defined as the distance between the peak of the normalized intensity distribution curve and the optical axis. During

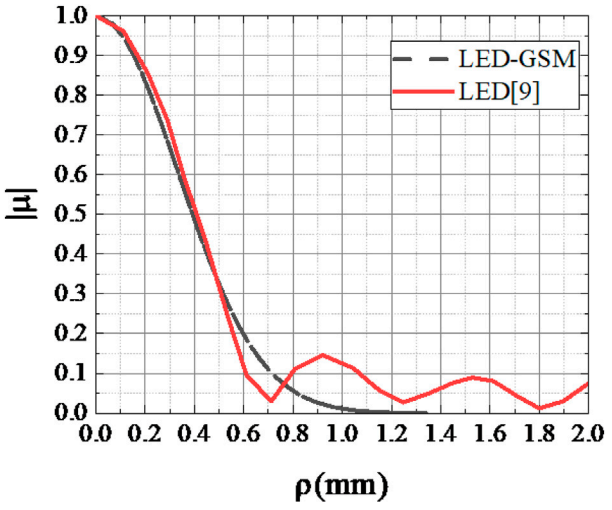

FIGURE 2
Comparison the results between LED-GSM model and experiment in a vacuum.

the transmission of partially coherent light, the ratio of the spatial coherence length to the beam radius is a constant [23], which means that

$$\alpha = \frac{\rho_0(z)}{w(z)} \tag{12}$$

From Equations 10, 11, it can be seen that in the transmission of LED-GSM beams, the spatial coherence length and beam width of the light field are related to the size of the light source and spatial coherence length, and they also vary with the increase of the transmission distance. In this paper, numerical analysis and experimental measurements of the LED-GSM beam transmission characteristics at different distances will be carried out. The effectiveness of LED-GSM will also be experimentally verified by using Equation 12.

3 Experimental verification of LED-GSM model

Regarding the validation of the narrow beam $\Phi_{1/2} \leq 10^o$ LED-GSM model, we first compared and verified it with the experimental results of the spatial coherence length of LED beams in Ref. [10]. Subsequently, we constructed experimental systems for obtaining spatial coherence and spot size of the narrow beam LED light field, using the Thorlabs LED528EHP model as the light source. We carried on a comprehensive model validation of the spatial coherence length and spot size of the LED light field at different distances.

3.1 Validation against literature comparison

Literature [10] provides the spatial complex coherence curve of a red LED chip with a central wavelength of 623.3 nm and a 3 mm square side of the light-emitting area. This curve exhibits a Sinc function distribution at the observation plane 5 m away, as shown by the red line in Figure 2. By utilizing Equations 6, 10, the spatial complex coherence curve of the LED-GSM ($w_s = 1.5\ mm$, $\sigma = 15\ \mu m$) follows a Gaussian function distribution, represented by the black dashed line in Figure 2. The good agreement at a spatial coherence length of $\rho_0(z=5) \approx 0.7mm$ on a 5 m observation plane.

3.2 Experimental verification of spatial coherence

The experiment used a Thorlabs LED528EHP green LED ($\lambda = 525nm, \Phi_{1/2} = 9^o$), whose emitted beam characteristics meet the conditions of the LED-GSM model. The LED is a system that packages a light-emitting chip and a focusing lens. The spatial coherence length and spot size of its light field were measured at different distances, and the measurement results were compared and analyzed with the simulation results given in Equations 10–12.

Measurement of spatial coherence of partially coherent light from a narrow beam LED is performed using Young's double-slit interference experiment, as shown in Figure 3A. As stated in Section 2.2, the distance between the LED-GSM light source plane and the LED source is z_1, determined by the condition of $\Phi_{1/2} \leq 10^o$ and $\mathbf{r}^2 \ll z_1^2$. Double slits are placed at a distance of z from the z_1 plane, and the interference pattern is determined by the parameters of the double slits, a and b, as well as the distance z. The typical interference pattern is a series of bright and dark fringes, as shown in Figure 3B. The intensity distribution of the interference fringes is detected using a high-sensitivity SG-11-01K40–00-R model linear CCD ($14\ \mu m \times 14\ \mu m$), as shown in Figure 3C.

In the experiment, to ensure consistency with theoretical calculations, the selected transmission distance and double-slit conditions in the optical path fall within the paraxial approximation range. It is assumed that the diffracted light emitted from points P_1 and P_2 combine at point Q to produce interference fringes, with the distance between the double slits being b. In the interference field of the double slits, the intensity of light at a particular point Q in space can be expressed as[24].

$$I(Q) = I_1(Q) + I_2(Q) + 2\sqrt{I_1(Q)I_2(Q)}\left|\mu_{12}(w)\right|\cos\beta_{12}(w) \tag{13}$$

Where $I_1(Q)$ and $I_2(Q)$ denote the intensities of the sub-waves at points P_1 and P_2, respectively, that give rise to the light intensity at point Q. $|\mu_{12}(w)|$ represents the spectral coherence between points P_1 and P_2, while $\beta_{12}(w)$ corresponds to the phase of $|\mu_{12}(w)|$, which continuously varies between $(0, 2\pi)$. Under the quasi-monochromatic approximation, the relationship between the visibility of interference fringes and the degree of coherence satisfies (T and J, 1982)

$$\gamma(Q) = \frac{(I_{\max} - I_{\min})}{(I_{\max} + I_{\min})} = \frac{2\sqrt{I_1(Q)I_2(Q)}}{I_1(Q) + I_2(Q)}\left|\mu_{12}\right| \tag{14}$$

Where $\gamma(Q)$ is the visibility of the interference fringes, and $|\mu_{12}|$ is the spatial complex coherence between two points. Under the assumption that a condition is satisfied with $I_1(Q) = I_2(Q) = I(Q)$

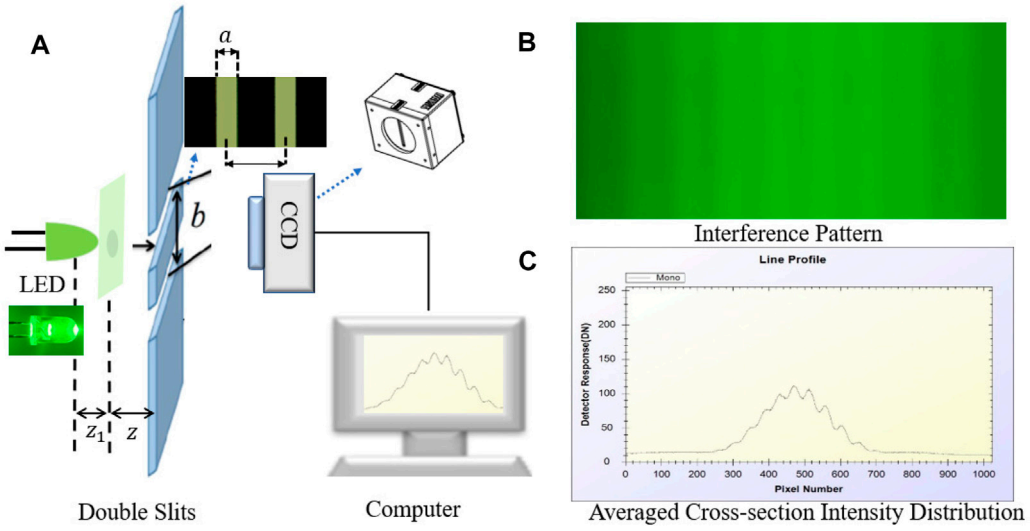

FIGURE 3
The experiment system. **(A)**Double slit. **(B)**Interference pattern. **(C)**Averaged cross-section intensity distribution.

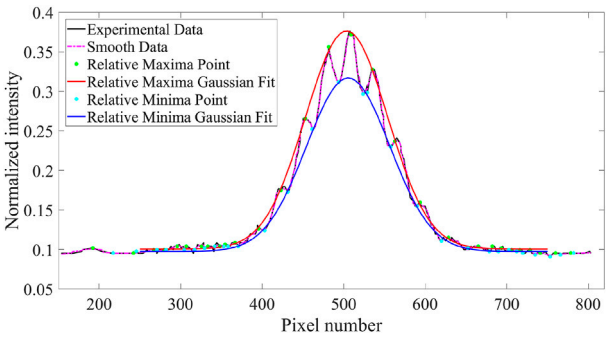

FIGURE 4
Diffraction patterns. The crest (maxima points) and trough (minima points) are represented by green and cyan marks, respectively. (z_1 = 0.1 *m*, z = 0.3 *m*, a = 0.06 *mm*, b = 0.2 *mm*).

TABLE 1 Double slits parameters.

No.	1	2	3	4	5
a \ *mm*	0.03	0.03	0.06	0.06	0.1
b \ *mm*	0.08	0.1	0.2	0.3	0.4

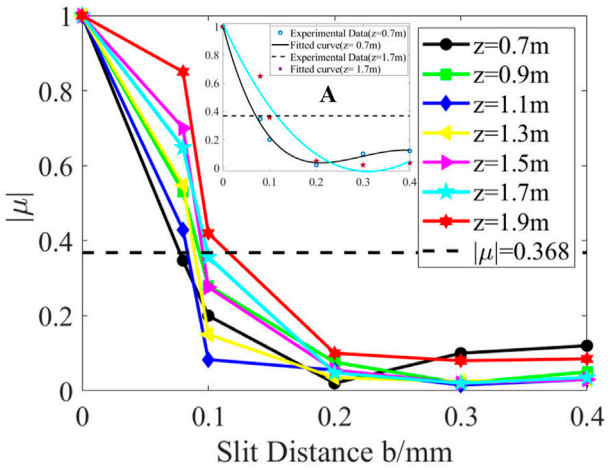

FIGURE 5
The curve of changes in $|\mu|$ at various distances due to variations in the double-slit parameters. **(A)** Simulation curve fitting experiment points.

[24], the visibility of $\gamma(Q) \approx |\mu_{12}|$ can be determined. Therefore, the spatial coherence of the light beam can be determined by measuring the maximum and minimum values of the interference fringe intensity.

Due to the influence of background light and other noise, there are errors in determining the accurate values of I_{max} and I_{min}. To address this, the Gaussian fitting of the maximum and minimum points of the interference fringes is considered, and the maximum value of each obtained Gaussian curve is taken as the respective values of I_{max} and I_{min}.

Figure 4 shows the interference pattern of the intensity of the interference fringes at $z = 0.3$ *m* after passing through the double slits (a = 0.06 *mm*, b = 0.2 *mm*). By normalizing and smoothing the collected interference fringes, removing background light and other noise, and fitting the two Gaussian envelopes of the interference fringes, the red and blue curves correspond to the Gaussian curves obtained using the maximum and minimum points, respectively. Therefore, I_{max} = 0.376 and I_{min} = 0.304 are determined and substituted into Equation 13 to calculate the spatial complex coherence value of the light field at the double slits, which is denoted as $|\mu|$ = 0.150.

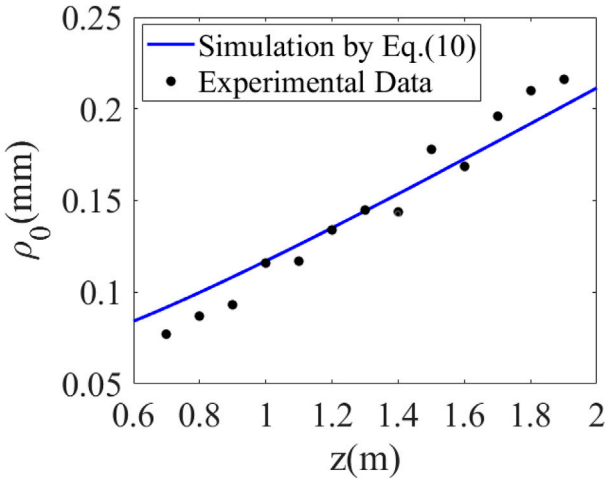

FIGURE 6
Determine the initial spatial coherence length of the model by means of simulation and experimental measurements. (z_1 = 0.1 *m*).

The experiment in this paper used 5 sets of double slits with different spacing, whose specific parameters are shown in Table 1. The widths of the double slits (a) and the separations between them (b) have been finely adjusted and customized based on actual conditions. Through repeated experimentation, clear interference fringes can be obtained to achieve the most accurate measurement of spatial coherence length. Based on the measurement method of Young's double-slit interference experiment introduced above, the spatial complex coherence of the optical field was measured using different double slits at different distances, and the relationship between the spatial complex coherence and the double-slit size was obtained. Figure 5 shows the relative spatial complex coherence curve relationship of the narrow beam LED at different double slit spacings, which are 0.7, 0.9, 1.1, 1.3, 1.5, 1.7, and 1.9 m, respectively. Although the number of experimental points is relatively small, the experimental measurement results in $z = 0.7m$ still show that the amplitude of spatial complex coherence of $|\mu|$ does not vary monotonically with the increase of the double slit separation b. This is because the amplitude of the spatial complex coherence of the light field generated by the LED circular disk source exhibits a Bessel function relationship with the variation of b, which also indicates the consistency between the experimental measurement results and the theoretical results in the trend of change. Due to the limited number of double slits used in the experiment, we can calculate the spatial coherence length of the LED at various light transmission distances by identifying the intersection point between the curve obtained from fitting the measurement points in Figure 5A and $|\mu| = 1/e$. For instance, by analyzing of $z = 0.7\ m$ and $z = 1.7\ m$, we can determine the spatial coherence of the LED source to be 77 μm and 110 μm.

Using the method described above, we can determine the spatial coherence length of the optical field at various distances. The results are shown in Figure 6, where the scattered points represent the experimental measurement results. Due to experimental constraints, measuring the spatial coherence length of the optical field at z_1 plane directly is not feasible. Nonetheless, we can use a combination of Equation 10 and experimental data, and optimize them using the least squares method to determine the spatial coherence length of $\sigma = 41\ \mu m$ at $z_1 = 0.1\ m$. At this juncture, the residual between the theoretical simulation and experimental measurement values is approximately ±0.02.

The observation plane of the light beam at $z_1 = 0.1\ m$ serves as the initial light source plane for the LED-GSM model. The value of $\sigma = 41\ \mu m$ obtained from this plane is substituted into Equation 9 to calculate the curves that illustrate the relationship between the spatial complex coherence amplitude $|\mu|$ and ρ at positions $z = 0.9\ m$ and $z = 1.9\ m$, respectively. These curves are represented by the blue curve in Figure 7. The simulation results of the LED-GSM model presented in Figure 7 exhibit good agreement with the experimental measurement results of the spatial complex coherence amplitude. Through the comparison between the LED-GSM model simulation results and experimental measurement results in Figure 7, it is not only demonstrated that the reliability of the initial light source plane obtained by optimizing the curve in Figure 6 is satisfactory, but also confirms the accuracy of the LED-GSM model.

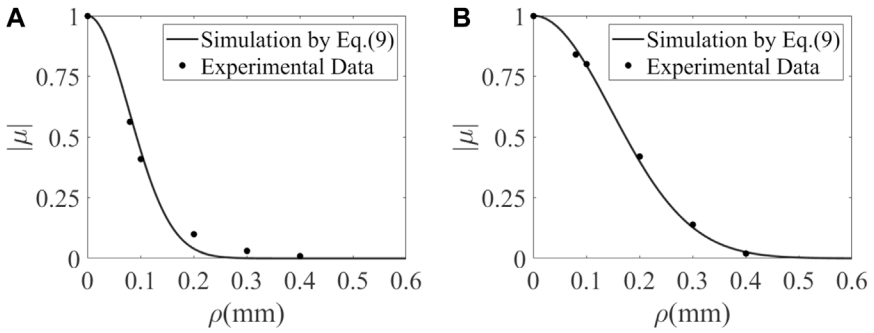

FIGURE 7
Simulation and experimental results comparing the variation of spatial complex coherence amplitude with respect to ρ. **(A)** $z = 0.9\ m$, $\sigma = 41\ \mu m$. **(B)** $z = 1.9\ m$, $\sigma = 41\ \mu m$.

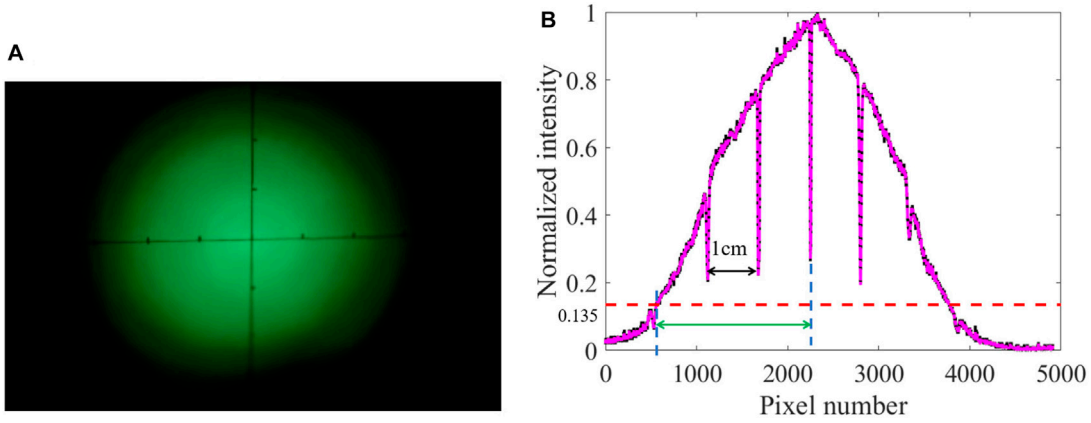

FIGURE 8
Experimental measurement results of spot radius. (z_1 = 0.1 *m*) **(A)** Spot pattern. **(B)** Fitting LED beam using Gaussian distribution.

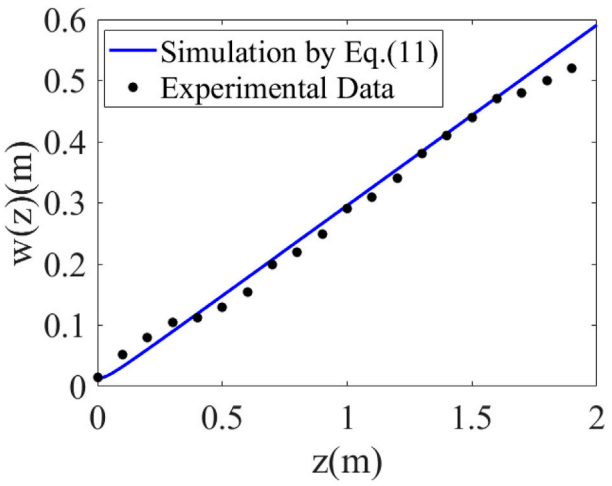

FIGURE 9
Simulation and experimental verification of spot radius. (z_1 = 0.1 *m*, σ = 41 μm).

TABLE 2 The ratio of experimentally measured spatial coherence length to spot radius.

z \ *m*	0.6	0.7	0.8	0.9	1.0	1.1	1.2
α \ 10^{-4}	3.85	3.95	3.75	4.00	3.77	3.94	3.81
z \ *m*	1.3	1.4	1.5	1.6	1.7	1.8	1.9
α \ 10^{-4}	3.59	3.80	4.00	3.60	4.00	4.10	4.01

Equation 11 indicates that the beam radius of $w(z)$ is related to the size of the light source of w_s and the spatial coherence length of σ. In this study, experiments were carried out on the narrow beam LED discussed in Section 3.2. The beam size was directly measured by taking photographs of the beam spot. A typical beam spot pattern (z_1 = 0.1 *m*) captured by a Nikon D800 DSLR camera (with a resolution of 7,360 × 4,912) is shown in Figure 8A.

The normalized intensity distribution is shown in Figure 8B, and the spot radius size is obtained using the equation of $w(z) = I(z)/e^2$, First, the calibrated pixel spot size is 6.5 μm, as shown in the black mark. Further, the effective spot radius can be calculated as 1.4 cm, as shown by the green mark. Similarly, the spot size can be obtained from $z = 0$ to $z = 1.9$ *m*, i.e., the spot size on the observation plane at different distances, as shown in Figure 9 for the discrete points.

By substituting σ = 41 μm into Equation 11 of the LED-GSM model, we can observe a curve of the beam radius increasing with distance. As shown in Figure 9, the beam radius obtained from the LED-GSM model simulation agrees well with the experimental measurements as the distance increases, and the error range of the simulation and experiment is within ±0.04 *m*. As shown in Equation 12, the ratio of the spatial coherence length to the beam radius is constant of α, regardless of the optical transmission distance. The value of $\alpha_{sim} = 3.60 \times 10^{-4}$ can be determined from the model simulation results. By combining the experimental measurements from Figure 6 and Figure 9, we can obtain the ratio of the coherence length to the spot radius as shown in Table 2, with a constant coefficient of $\alpha_{\exp} = 3.86 \times 10^{-4}$. Thus, considering the margin of error, it can be concluded that $\alpha_{sim} \cong \alpha_{\exp}$, implies that the ratio of α is associated with the parameters of the light source and transmission distance. This finding is consistent with the rule derived from Friberg's study on GSM beam vacuum transmission (T and J, 1982). Additionally, it provides further evidence that the coherence length of the light source plays a crucial role in determining the spot radius.

4 LED-GSM long-distance transmission characteristics

A simulation study was conducted on the partial coherence transmission characteristics of LED optical fields in long-distance optical transmission for narrow-beam LED optical communication applications. Using Equations 10, 11, the far-field coherence length and beam radius of the LED-GSM source

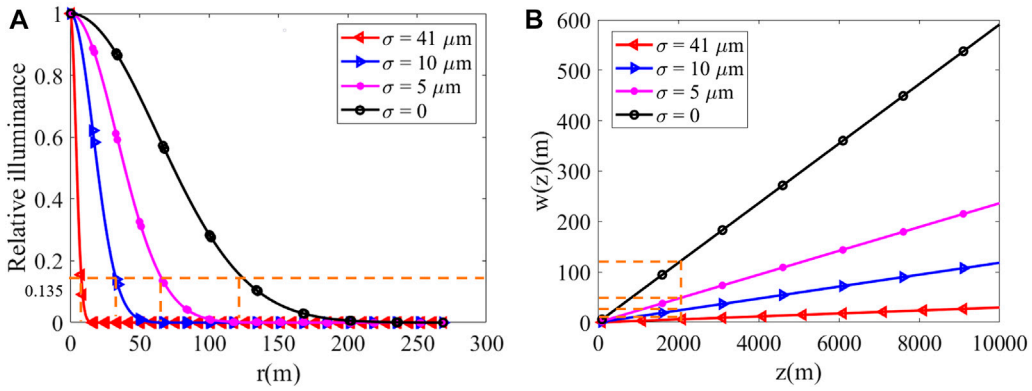

FIGURE 10
Variation in relative intensity distribution and beam radius with different σ. **(A)** Relative intensity vs. r (z = 2,000 m). **(B)** Beam radius vs. z.

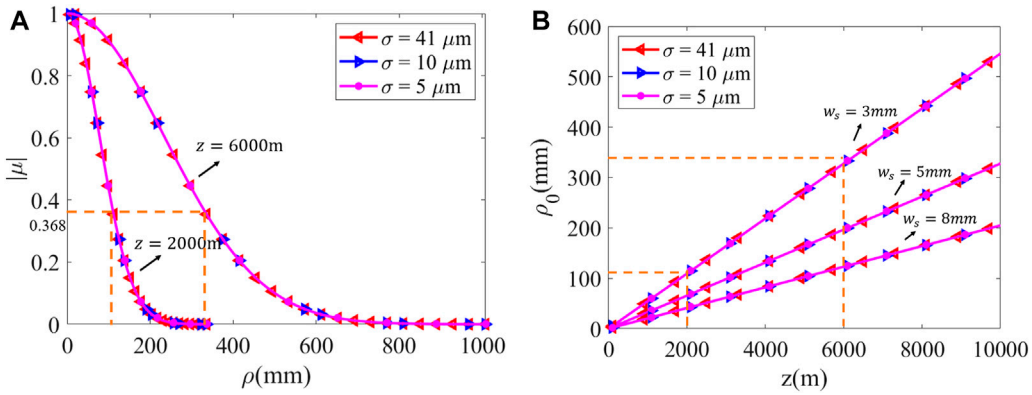

FIGURE 11
Changes in the amplitude of spatial complex coherence and the spatial coherence length at different values of σ. **(A)** $|\mu|$ vs. ρ (w_s = 3 mm). **(B)** ρ_0 vs. z.

was simulated and calculated at different spatial coherence lengths on the LED source plane, showing how they change with distance. Simulation parameters $\lambda = 525\,nm$, $w_s = 3\,mm$, α with values of 0, 5 μm, 10 μm and 41 μm taken separately. Here, $\sigma = 0$ corresponds to the case where the LED source is considered as fully incoherent light, with a transmission distance up to 10,000 m.

Figure 10A illustrates the correlation between the normalized intensity distribution on the observation plane and the increasing spot radius. The figure demonstrates that the normalized light intensity distribution is significantly influenced by the size of σ, and the spot size at the normalized intensity of $1/e^2$ is utilized to ascertain the beam radius. When considering the spatially coherent lengths mentioned above, the resulting beam radii are 65.75, 33.13, and 7.89 m respectively. These radii decrease as the corresponding length of σ increases. In the case of fully incoherent light, the beam radius is 123.61 m, which differs from the beam radius while σ = 41 μm at 15 times. It is evident that, for a specific outgoing power of an LED light source, after undergoing the same channel attenuation, the partial coherence of the light source increases, resulting in a smaller spot size and an order of magnitude increase in power density on the observation plane. This highlights the impact of spatial partial coherence on the transmission characteristics of the LED light source. The underlying reason for this phenomenon is that the beam with partial coherence possesses a degree of randomness in its original wavefront. Figure 10B depicts the relationship between beam radius and transmission distance z for various values of σ. It is evident from the figure that the beam radius reduces as σ increases, and the dashed line in the figure corresponds to that in Figure 10A. In addition, the beam radius linearly increases with transmission distance, consistent with the pattern of beam radius variation reported in literature [25] for 1D linear GSM beams with increasing coherence length in a vacuum. The rate of beam expansion is dependent on the spatial coherence length σ of the source; a smaller spatial coherence length results in faster beam radius expansion. This is due to the influence of transmission distance causing free diffraction-induced beam expansion.

Figure 11 depicts the relationship between the complex degree of coherence $|\mu|$ and spatial coherence length ρ_0 with respect to transmission distance for different spatial coherence lengths of σ.

The curves of $|\mu|$ *versus* ρ on the observation plane at 2,000 m and 6,000 m are shown in Figure 11A. It is evident from the curves that the $|\mu|$ curves overlap when σ is 41 μm, 10 μm and 5 μm, respectively. The values of ρ_0 are 109 mm and 327 mm, respectively, at the observation planes of z = 2,000 m and 6,000 m. This is attributed to the free diffraction-induced beam expansion that occurs during beam transmission through the vacuum, resulting in increased variation in coherence length affected by the beam expansion. Nevertheless, the alteration in spatial coherence length ρ_0 is also impacted by the size of the source and transmission distance, as illustrated in Figure 11B. Figure 11B illustrates the relationship between coherence length, denoted as ρ_0, and its variation with respect to distance of z for different values of w_s. The figure shows that at a transmission distance of 2,000 m, the spatial coherence lengths corresponding to different σ values in Figure 11A are equal. When the transmission distance is increased to 6,000 m, the coherence lengths for w_s values of 3, 5, and 8 mm are 327, 196, and 122 mm, respectively. At this point, ρ_0 for $w_s = 3\ mm$ is roughly three times that of $w_s = 8\ mm$.This indicates that as the value of w_s decreases, the corresponding change in ρ_0 becomes more rapid, while ρ_0 exhibits a linear increase with respect to transmission distance. The reason is that when a beam of light is transmitted over long distances in a vacuum, as shown in Equation 10, the impact of the light source parameters on light transmission relative to spatial coherence dominates. Within this distance, the main mechanism of the light beam is free diffraction, leading to an expansion of the beam and an increase in the coherence length.

5 Conclusion

This paper is based on the generalized higher-order Lambert model and proposes the LED-GSM model for LED beams with a half-angle of no more than 10° in the region surrounding the light source plane. The validity and accuracy of the LED-GSM model are preliminarily verified by comparing the spatial complex coherence curves obtained from experiments with the approximate LED source model in reference (Lin H and M, 2012). This comparison supports the application of cross-spectral density transfer theory for studying the propagation of LED beams. Secondly, the spatial coherence length and spot size are measured experimentally at different distances using the Thorlabs LED528EHP model light source. The results show good agreement with those corresponding to the theoretical simulation of LED-GSM beam transmission at CSDF, thereby verifying the validity of the proposed LED-GSM model. Finally, by carrying out a study of the long-distance transmission characteristics of the LED-GSM model, it was found that the far-field beam radius decreases significantly with the increase of σ on the LED-GSM light source plane, and the spatial complex coherence amplitude remains unchanged but is distinctly different from the fully incoherent light of σ = 0. In particular, the spatial coherence length on the observation plane can reach tens to hundreds of millimeters at transmission distances of several kilometers. With increasing distance, the spatial coherence length increases significantly linearly, especially as w_s = 8 mm decreases to w_s = 3 mm, where ρ_0 on the observation plane at z = 6,000 m is about three times larger than at z = 2,000 m.

The results presented above can be utilized to solve problems related to near-range holographic displays, interferometry, and the design of long-distance atmospheric light detection and communication systems. They also offer a valuable mathematical theoretical analysis of LED atmospheric transmission, providing a dependable theoretical basis for the development of outfield experiments. Moreover, this study addresses the limitation of treating LEDs as a fully incoherent light source during long-distance light transmission. It establishes a theoretical framework for investigating the impact of attenuation, scattering, atmospheric turbulence, and ambient light interference on narrow-beam LED arrays during long-distance optical transmission channels.

Data availability statement

The original contributions presented in the study are included in the article/Supplementary Material, further inquiries can be directed to the corresponding authors.

Author contributions

XH and ZM proposed the project. ZM and FL conducted the equation derivation, simulation, ZM and PZ conducted experimental research and image processing. ZM and XH wrote the manuscript. FL and QL helped to modify the documentation. All authors reviewed the manuscript. All authors contributed to the article and approved the submitted version.

Funding

This work was supported by the Fundamental Research Funds for the Central Universities (ZYTS23077, ZYTS23073).

Conflict of interest

The authors declare that the research was conducted in the absence of any commercial or financial relationships that could be construed as a potential conflict of interest.

Publisher's note

References

1. Eduard Z. Analysis and experiment of wireless optical communications in applications dedicated to mobile devices with applicability in the field of road and pedestrian safety. *Sensors (Basel)* (2022) 22:1023. doi:10.3390/s22031023

2. Feng R, Yanyan C, Xurui M. Beam tracking algorithm for marine applications using visible light communication. *Appl Opt* (2020) 59:6751–9. doi:10.1364/ao.394597

3. Lim S, Jeon H, Ahn S, Hahn J. Optimal spatial coherence of a light-emitting diode in a digital holographic display. *Appl Sci* (2022) 12:4176. doi:10.3390/app12094176

4. Khaidarov ELZ, Paniagua-Domínguez R, Ha ST, Valuckas V, Liang X, Akimov Y, et al. Controlof led emission with functional dielectric metasurfaces. *Laser Photon Rev* (2020) 14:1900235. doi:10.1002/lpor.201900235

5. Srisuphaphon S, Buathong S, Deachapunya S. Realization of an optical vortex from light-emitting diode source by a vortex half-wave retarder and using talbot effect based detection. *Opt Laser Tech* (2022) 1:107746. doi:10.1016/j.optlastec.2021.107746

6. Chen GTH, Lin H, Chen Z, Pu J. Spectral spatial coherence of high-power multi-chip leds. *Optoelectronics Lett* (2012) 8:422–5. doi:10.1007/s11801-012-2322-6

7. Deng Y, Chu D. Coherence properties of different light sources and their effect on the image sharpness and speckle of holographic displays. *Scientific Rep* (2017) 7:5893. doi:10.1038/s41598-017-06215-x

8. Xie G, Chen M, Mazilu M, Zhang S, Bansal A, Dholakia K, et al. Measuring and structuring the spatial coherence length of organic light-emitting diodes. *Laser Photon Rev* (2016) 10:82–90. doi:10.1002/lpor.201500065

9. Mehta D, Saxena K, Dubey SK, Shakher C. Coherence characteristics of light-emitting diodes. *J Lumin* (2010) 130:96–102. doi:10.1016/j.jlumin.2009.07.027

10. Lin H, Hua T, Meng H, Ji-Xiong P. Measuring and structuring the spatial coherence length of organic light-emitting diodes. *Acta Optica Sinica* (2012) 32:7. doi:10.3788/AOS201232.0323003

11. Zmija A, Deiml P, Malyshev D, Zink A, Anton G, Michel T, et al. Led as laboratory test source for astronomical intensity interferometry. *Opt Soc America* (2020) 28:5248–56. doi:10.1364/OE.28.005248

12. Li Z, Qiu G, Zhao L, Jiang M. Dual-mode led aided visible light positioning system under multi-path propagation: Design and demonstration. *IEEE Trans Wireless Commun* (2021) 20:5986–6003. doi:10.1109/TWC.2021.3071469

13. Nixon M, Redding B, Friesem AA, Cao H, Davidson N. Efficient method for controlling the spatial coherence of a laser. *Opt Lett* (2013) 38:3858–61. doi:10.1364/OL.38.003858

14. He Q, Turunen J, Friberg AT. Propagation and imaging experiments with Gaussian schell-model beams. *Opt Commun* (1988) 67:245–50. doi:10.1016/0030-4018(88)90143-5

15. Carter WH, Wolf E. Coherence properties of lambertian and non-lambertian sources. *J Opt Soc America* (1975) 65:1067–71. doi:10.1364/JOSA.65.001067

16. Wang Q, Zhang K, Lin D, Liang X, Liu Y, Zhang S, et al. Introducing an n-type electron deceleration layer to enhance the luminous efficiency of algan-based duv-leds. *Front Phys* (2023) 11:1118946. doi:10.3389/fphy.2023.1118946

17. Jacobs VFS, Rombauts P, Hanselaer P. Near-field and far-field goniophotometry of narrow-beam led arrays. *Lighting Res Tech* (2015) 47:470–82. doi:10.1177/1477153514530139

18. Lu W, Liu L, Sun J, Yang Q, Zhu Y. Change in degree of coherence of partially coherent electromagnetic beams propagating through atmospheric turbulence. *Opt Commun* (2007) 271:1–8. doi:10.1016/j.optcom.2006.09.058

19. Yang H, Bergmans JWM, Schenk TCW, Linnartz JPMG, Rietman R. An analytical model for the illuminance distribution of a power led. *Opt express* (2008) 16:21641–6. doi:10.1364/OE.16.021641

20. Duarte FJ, Liao L, Vaeth KM. Coherence characteristics of electrically excited tandem organic light-emitting diodes. *Opt Lett* (2005) 30:3072–4. doi:10.1364/OL.30.003072

21. Emil W. *Introduction to the theory of coherence and polarization of light*. Cambridge: Cambridge University Press (2007).

22. Foley JT, Zubairy MS. The directionality of Gaussian schell-model beams. *Opt Commun* (1978) 26:297–300. doi:10.1016/0030-4018(78)90205-5

23. Friberg AT, Sudol RJ. Propagation parameters of Gaussian schell-model beams. *Opt Commun* (1982) 41:383–7. doi:10.1016/0030-4018(82)90161-4

24. Craford MG, Holonyak N, Kish FA. In pursuit of the ultimate lamp. *Scientific Am* (2001) 284:62–7. doi:10.1038/scientificamerican0201-62

25. Zhou P, Liu Z, Xiaojun X, Xiaolin W, Li X, Chen Z. Influence of turbulent atmosphere on the far-field coherent combined beam quality. *Chin Opt Lett* (2008) 6:625–7. doi:10.3788/col20080609.0625